Journal of
Microscopy

Journal of Microscopy, Vol. 256, Issue 3 2014, pp. 237–247
Received 4 June 2014; accepted 10 August 2014
doi: 10.1111/jmi.12179

High resolution SEM imaging of gold nanoparticles in cells and tissues

A. GOLDSTEIN*, Y. SOROKA*, M. FRUŠIĆ-ZLOTKIN*, I. POPOV† & R. KOHEN*
*Institute for Drug Research, School of Pharmacy, Faculty of Medicine, The Hebrew University of Jerusalem, Jerusalem, Israel
†The Harvey M Krueger Center for Nanoscience and Nanotechnology, The Hebrew University of Jerusalem, Jerusalem, Israel

Key words. charging effects, conductive coating, gold nanoparticles, high resolution scanning electron microscopy, keratinocytes, macrophages, skin penetration.

Summary

The growing demand of gold nanoparticles in medical applications increases the need for simple and efficient characterization methods of the interaction between the nanoparticles and biological systems. Due to its nanometre resolution, modern scanning electron microscopy (SEM) offers straightforward visualization of metallic nanoparticles down to a few nanometre size, almost without any special preparation step. However, visualization of biological materials in SEM requires complicated preparation procedure, which is typically finished by metal coating needed to decrease charging artefacts and quick radiation damage of biomaterials in the course of SEM imaging. The finest conductive metal coating available is usually composed of a few nanometre size clusters, which are almost identical to the metal nanoparticles employed in medical applications. Therefore, SEM monitoring of metal nanoparticles within cells and tissues is incompatible with the conventional preparation methods. In this work, we show that charging artefacts related to non-conductive biological specimen can be successfully eliminated by placing the uncoated biological sample on a conductive substrate. By growing the cells on glass pre-coated with a chromium layer, we were able to observe the uptake of 10 nm gold nanoparticles inside uncoated and unstained macrophages and keratinocytes cells. Imaging in back scattered electrons allowed observation of gold nanoparticles located inside the cells, while imaging in secondary electron gave information on gold nanoparticles located on the surface of the cells. By mounting a skin cross-section on an improved conductive holder, consisting of a silicon substrate coated with copper, we were able to observe penetration of gold nanoparticles of only 5 nm size through the skin barrier in an uncoated skin tissue. The described method offers a convenient modification in preparation procedure for biological samples to be analyzed in SEM. The method provides high conductivity without application of surface coating and requires less time and a reduced use of toxic chemicals.

Correspondence to: Alona Goldstein, The Hebrew University of Jerusalem, Institute for drug research, School of Pharmacy, Israel. Fax: 972-2-6757246; e-mail: alona.goldstein@gmail.com

Introduction

In the recent years, gold nanoparticles (AuNPs) are widely investigated as a diagnostic and therapeutic tool in medical applications, due to their biocompatibility and their unique physical and optical properties (Dreaden *et al.*, 2012). Interaction of AuNPs with living cells includes adsorption, uptake and internal localization. It depends on the nanoparticle size, shape and surface chemistry, as well as on the cell type (Levy *et al.*, 2010). These properties also affect the penetration of AuNPs into biological tissues (Sonavane *et al.*, 2008). Penetration of metallic nanoparticles into skin is important as a way of topical drug delivery, yet challenging due to the presence of the highly impermeable uppermost layer of the skin *stratum corneum*. Skin permeability may be improved by chemical procedures, such as PEG (Polyethylene Glycol) coating (Ryman-Rasmussen *et al.*, 2006) or by physical methods, such as stripping, chemical peeling, electrophoresis and micro-needles (Prausnitz *et al.*, 2004).

Visualization of gold nanoparticles interaction with cells and tissues requires high resolution imaging techniques due the small size of the metal nanoparticles. Individual nanoparticles are not distinguishable with conventional optical microscopy since their size is below the resolution limit. Dark field microscopy takes advantage of the surface plasmon excitation of gold nanoparticles and is used in the imaging of cancer cells through functionalized nanoparticle–receptor binding on to cell surface biomarkers (Huang *et al.*, 2007). Yet, individual nanoparticle of several nanometres cannot be distinguished from the scattering background of the cells. Transmission electron microscopy (TEM) is a powerful tool that allows observation of a single nanoparticle inside cellular compartments and is widely used for the intracellular detection of metallic nanoparticles. However it requires a rather complicated and time consuming sample preparation while each sample

shows highly local space limited information from a sliced cell (Schrand *et al.* 2010). New generation of High Resolution SEM (HRSEM) allows a resolution better than 1 nm, approaching the resolution of TEM. With this technique, it is possible to analyze interactions such as the adsorption and uptake of metallic nanoparticles by cells (Plascencia-Villa *et al.*, 2013). HRSEM combines the advantages of a much simpler sample preparation and higher depth-of-field imaging thus providing a semi-3D information on the morphology and cell structure. A complete 3D information, including subcellular structure, can be achieved by the relatively new and sophisticated technique of serial block face SEM (SBF-SEM) that was first introduced by Denk *et al.* in 2004 (Denk & Horstmann, 2004), now available commercially, and expected to evolve into a mainstream technique in the next few years (Hughes *et al.*, 2013). In this technique, an ultramicrotome is integrated within the chamber of the SEM and a diamond knife removes a thin slice from the resin-embedded sample between each BSE imaging cycle. Using this technique it is possible to quantify the dose of NPs inside the cell and map their 3D distribution (Summers *et al.*, 2013). Nevertheless this technique requires special tooling, extensive expertise, time consuming and a rather complex sample preparation procedure, similar to TEM.

The resolution in SEM image is highly dependent on the quality of the biological sample. Conventional sample preparation for HRSEM includes chemical fixation, postfixation in osmium tetroxide, dehydration and coating with a thin metal layer. Freezing methods are also used to provide superior ultrastructure compared to chemical fixation (Schatten, 2010). Dehydration of biological specimen has diverse protocols, depending on specimen size, porosity and the internal or external features to be examined. The role of all the methods is to remove or immobilize water in order to maintain the structural integrity of the specimen in the vacuum of the electron microscope (Goldstein, 1981). Staining by osmium tetroxide is recommended for high magnifications, since it provides contrast to the plasma membrane as a lipid stain and also improves conductivity by embedding a heavy metal into cell membranes (Brunk *et al.*, 1980). Coating is commonly applied to increase the conductivity of the naturally insulating biological sample. Without coating, negative charge accumulates within the scanned area of the insulating material and creates local electrical fields that can defocus or deflect the electron beam and especially interfere with the collection of low energy secondary electrons (Joy & Pawley, 1992). Typically a thin metal coating is applied to reduce the effects of charging. However, if too thick, the coating may hinder small details on the specimen. Conversely, if too thin, it becomes discontinuous and decorates the specimen (Peters, 1986).

There are several techniques other than metal coating to prevent charging effects. One of them is the low vacuum operation, also called variable-pressure mode or environmental SEM. In this technique, the electron beam passes through a low concentration of gas that neutralizes the surface charge (Robinson, 1975). Nevertheless this technique is less suitable for the detection of nanoparticles due to its reduced contrast and resolution. Another technique is the low voltage operation, where the charge introduced by the primary electron beam is just balanced by the BSE and SE emitted from the sample (Joy & Joy, 1991). This method however is less suitable for BSE mode imaging due to the low BSE signal obtained at such low voltages. Staining by heavy metals is also commonly used as a method to prevent charging. However, since they serve as contrast agents, their distribution is nonuniform, leaving regions without sufficient draining of the charge and the result is inferior contrast in BSE imaging compared with coated samples (Titze & Denk, 2013).

An alternative approach to eliminate charging effects was applied in the study of gold nanoparticles adsorption on unstained and uncoated cancer cells (Hartsuiker *et al.*, 2011). Cells were grown on a glass precoated with a thin gold layer. After fixation cells were incubated with AuNPs, followed by dehydration and imaging without staining or coating. This protocol gave sufficient resolution for imaging of 40 nm AuNPs adsorbed to the surface membrane of the cells. In another research, the uptake of star-shaped gold nanoparticles by macrophages was studied using FESEM (Plascencia-Villa *et al.*, 2013). In this study, macrophages were mounted onto a silicon wafer after fixation and dehydration, without staining or coating the cells. Their protocol allowed observation of 80 nm gold nanoparticles, internalized by macrophages.

In our study, we demonstrate the ability to minimize charging effects and obtain high resolution SEM images of 10 nm gold nanoparticles, internalized by macrophages and keratinocytes cells, by growing the cells on top of conductive coated holders, without the need for staining or coating the cells. In addition, a procedure was defined for the application of a conductive holder to the study of 5 nm gold nanoparticles penetration into skin organ culture, without subsequent coating.

Methods and materials

Fine chemicals were purchased from Sigma-Aldrich (Rehovot, Israel), unless otherwise stated. Cell culture media supplies were obtained from Biological Industries, Beit Haemek, Israel. The media used, RPMI and DMEM, were supplied with 2 mM L-glutamine, 100 U/mL penicillin, 100 μg/mL streptomycine and 10% fetal bovine serum (FBS). 10 nm and 30 nm diameter gold nanoparticles, 1E13 particles/mL, in citric acid solutions, were kind gift from Prof. Douglas. 5 nm diameter gold nanoparticles, 5.5E13 particles/mL, stabilized suspension in citrate buffer, were purchased from Sigma-Aldrich (Rehovot). Sputtering was carried out using 99.99% targets of chromium, tantalum, copper and tungsten/titanium 90/10 alloy at AVX Israel Ltd.

Cell growth on thin metal layers

Glass cover slips, 2 cm in diameter, 0.2 mm thick, (Marienfeld №1, Germany) were coated by 50 nm thin metal layer using DC magnetron sputtering technique in MRC943 machine. The following metals were deposited: tantalum (Ta), chromium (Cr), tungsten/titanium 90/10 alloy (W/Ti) and copper (Cu). Uncoated glass cover slips were used as a reference. Five replicates were prepared for each substrate. The samples were wiped with IPA Pharma wipes (Dr Fisher, Israel), placed in 6-well cell culture dishes and further sterilized by exposure to the UV lamp in a biological hood for 20 min. In order to improve cell adhesion, 120 μL of FBS was applied to the surface of each sample for 60 min. Then 0.24×10^6 cells of murine macrophages RAW 264.7 were seeded into each well in 2 mL RPMI medium and incubated at 37°C in 5% CO_2 atmosphere.

Cell viability was evaluated by determination of mitochondrial activity after 48 h, using the MTT colorimetric assay (Mosmann, 1983). Briefly, samples with macrophages grown as described above were transferred into wells containing 1.15 mL of 0.5 mg/mL (3–4,5-dimethylthiazol-2–yl)-2,5-diphenyltetrazolium bromide (MTT), and incubated for 30 min at 37°C. The resulting precipitated stain was extracted in 1 mL isopropanol for 5 min at room temperature with shaking. 100 μL aliquots were transferred to a 96-well plate where optical density at 570 nm, proportional to cell viability, was measured by a microplate reader (Synergy HT, BioTek, Winooski, USA).

Sample preparation of cells for HRSEM

Cells were grown on glass coated with 50 nm chromium as described previously. Two types of cells were grown: macrophages RAW 264.7 in RPMI medium and HaCaT, a human keratinocytes cell line, in DMEM. After the incubation time of 24–48 h, gold nanoparticles were added to the medium and incubated for 0.5–22 h. Then the samples were rinsed twice in PBS, fixed by 4% paraformaldehyde (PFA) in PBS for 15 min and kept at 4°C overnight. Dehydration was performed according to ethanol-freon protocol: two washes in PBS and gradual dehydration in serial changes of ethanol in H_2O for 2 min each (25%, 50%, 75% and twice 100%). Then ethanol was gradually substituted by freon with increasing freon concentrations, for 2 min each: 25%, 50%, 75% and twice 100%. Afterwards, samples were air-dried for 30 min at atmospheric pressure in a chemical hood and stored at dry atmosphere until visualization by SEM.

Sample preparation of tissue for HRSEM

Pieces of skin organ culture 0.5 × 0.5 cm were smear with 2 μL of dispersion of 5–10 nm gold nanoparticles, topically or through the medium for 24 h. At the end of the incubation period, samples were fixed in 4% PFA at 4°C, cryoprotected overnight in 20% sucrose in PBS and then frozen in the optimal cutting temperature compound (O.C.T., Tissue-Tek Sakura, Torrance, CA, USA). Frozen blocks were cut by LEICA CM1850 microtome to 8–15 μm thick sections which were placed on glass slides coated with a 50 nm chromium layer. Treating the chromium coated microscope slide with 10% FBS improved tissue adhesion to the slides and prevented tissue loss in subsequent procedures. Samples were dehydrated by ethanol-freon procedure or by ethanol-CPD (Critical Point Drying) procedure.

In an alternative dehydration procedure, tissues were placed directly on top of the chromium layer and dried at 60°C for 72 h, skipping the ethanol-freon procedure. In order to additionally reduce the charging of the samples, special holders with a much higher conductivity were prepared by sputtering of a thick 1 μm copper layer on a silicon semiconductor substrate.An adhesion layer of 50 nm chromium was sputtered between the Si substrate and the copper.

HRSEM

Observation of the samples was carried out in Extra High Resolution SEM (XHRSEM) Magellan^{TM} 400L (FEI Company, Hillsboro, OR, USA). This tool allows a resolution better than 1 nm, depending on the sample. The samples were attached to aluminium stubs using carbon tape. A conductive bridge of silver paste was made between the stub and the upper conductive surface of the samples. Images were taken in back-scattered electrons (BSE mode) with a vCD detector or in secondary electrons (SE mode) with a TLD detector at working distances 4–5 mm, accelerating voltage 5 kV and beam current 50 pA.

Results and discussion

Cell growth on thin metal layers

The viability results by MTT assay (Fig. 1) show that the cell growth on Ta, Cr and W/Ti was comparable to the values obtained for the conventional glass substrate. The confluence of the cells after 48 h was approximately 70% on the metals, similar to the coverage on the glass reference. Cu was found to be toxic to the cells. After 24 h the copper layer has been entirely dissolved from the glass into the medium and all the cells died, including those attached to the polystyrene bottom of the well around the coated sample.

Metallic coatings such as Cr, W, Au, Ti and Al have good biocompatibility (Bogner *et al.*, 2006), whereas Cu toxicity was reported on HL60 cells (Wolbers *et al.*, 2006) and Caco-2 cells (Bogner *et al.*, 2006). Metals with low mobility, such as Cr, Ta and W, are the most suitable coatings for high resolution SEM imaging due to their very fine morphology and their ability to form a continuous coating at a very low layer thickness. The thin coating has the advantage of minimal interaction with the

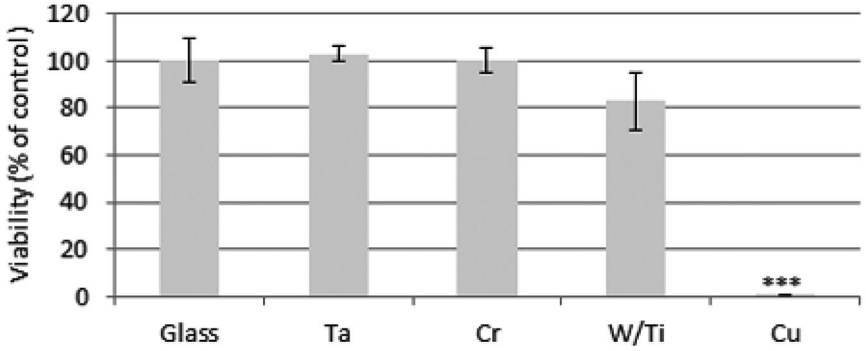

Fig. 1. Cell viability of macrophages growing on different metal coatings over 48 h, determined by MTT assay. The results are normalized to cultures growing on the glass substrate defined as 100% and presented as mean value ± SE. ***indicates significance of $p < 0.05$.

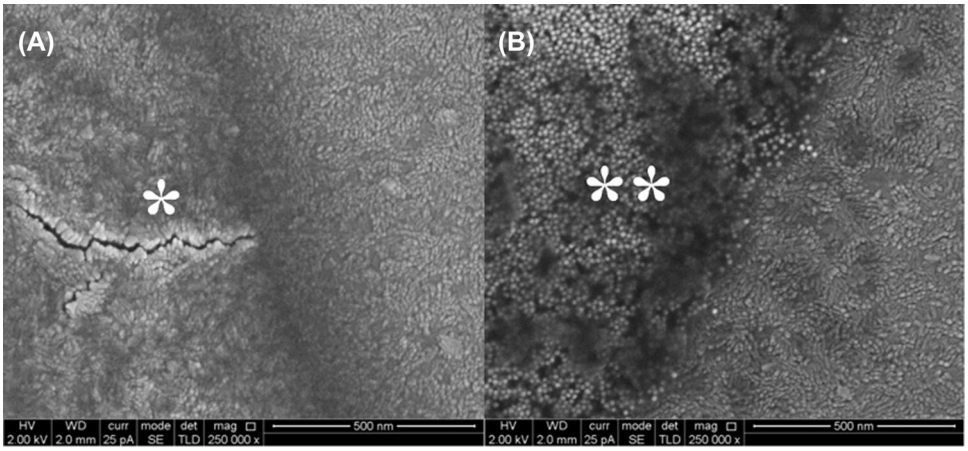

Fig. 2. (A) SE image of Cr coating on top of a dried droplet of 10 nm gold nanoparticles (left-hand side) on glass (right-hand side). Cracks appear on the coating over the dried droplet (*). The nanometric morphology of the Cr coating has grain size of 10 nm, obscuring the NPs below. (B) SE image of a dried droplet of 10 nm gold nanoparticles (left-hand side) placed on top of 50 nm Cr coating on glass (right-hand side). Spherical gold nanoparticles (**) are easily distinguished from the grains of the Cr coating.

electron beam in SEM and the fine morphology makes it possible to observe finer features in the sample (Peters, 1986). In our setup, where the conductive coating serves as a substrate for cell growth, the thin metal coating has the advantages of good conductivity with minimal surface roughness and semi-transparent optical characteristics. Transparent conductive coating opens the possibility for correlative microscopy. Indium tin oxide, a transparent conductive oxide, was studied as a potential coating for glass slides for cell cultures imaging by light and electron microscopy (Pluk *et al.*, 2008) and is implemented in recent studies (Rouvinski *et al.*, 2014). However, Indium tin oxide has major drawbacks such as high cost of production and relatively coarse morphology. Ultrathin transparent chromium layers of several nanometres were studied in the application of transparent metal contacts in optoelectronic devices (Rajani *et al.*, 2010). In our study, we applied thicker metallic layers of 50 nm, in order to achieve better electrical conductivity. Nevertheless, it was still possible to observe the cells in the transmission light microscope through the partially transparent layers. The Cr layer was chosen as a substrate for our next experiments, due to considerations of low price and availability, as well as its lower sheet resistance (9.8 Ω/sq compared with 13 Ω/sq for W/Ti and 30 Ω/sq for Ta).

Application of conductive Cr layer on glass for HRSEM imaging of 10 nm gold nanoparticles

We studied applicability of 50 nm thick conductive Cr layer for HRSEM by imaging 10 nm size gold nanoparticles on a glass. Figure 2 shows HRSEM images acquired under the same imaging conditions at drop-cast samples of gold nanoparticle dispersion: (i) deposited on a glass and then coated by Cr (Fig. 2A) and (ii) deposited on a glass precoated by Cr layer (Fig. 2B). Both images show very similar regions of the outer ring of a dried droplet. The chromium film has elongated grains with a typical grain size of 10 nm. In both cases, presence of conductive Cr on a glass sufficiently improved image quality

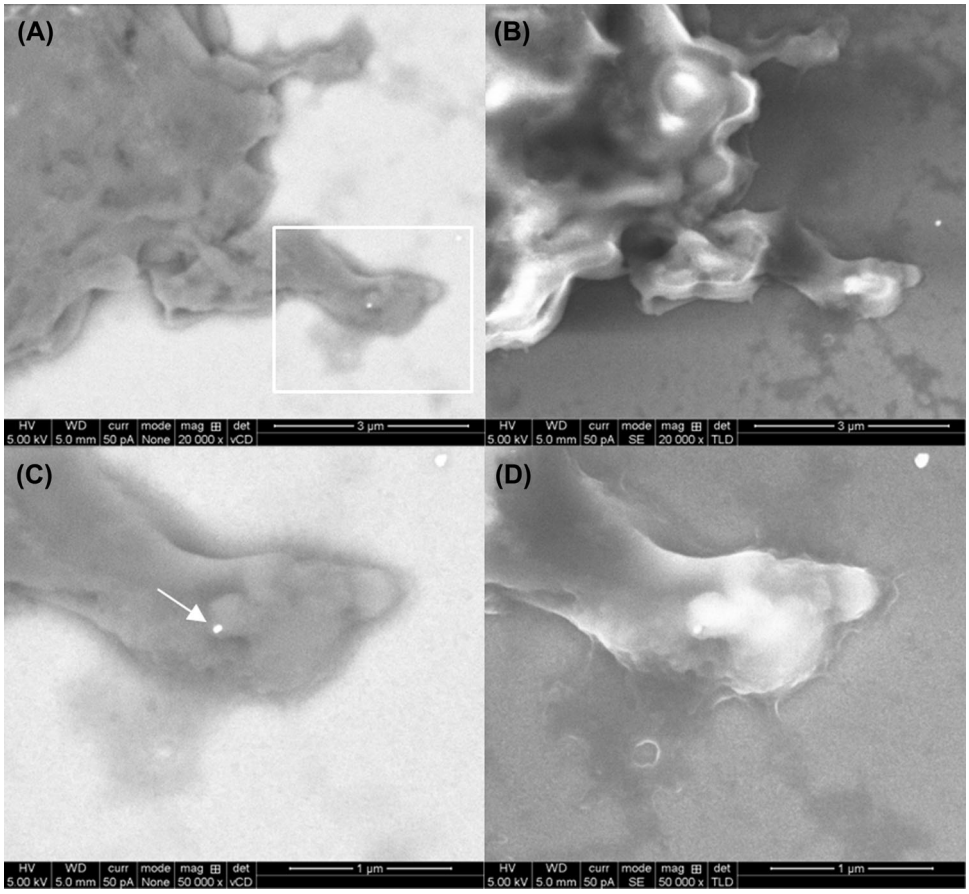

Fig. 3. HRSEM micrograph of a macrophage incubated with 1% dilution of 30 nm-sized gold NPs over 2 h on glass coated with Cr 50 nm layer. Images 'A' & 'B' were acquired in SE & BSE modes simultaneously. Images 'C' & 'D' are enlargements of the ROI marked in image 'A' with a rectangle. A 30 nm sized gold nanoparticle is indicated by an arrow in image 'C'.

due to decreasing of charging. But, as is clearly seen on Figure 2(A), coating with 50 nm Cr layer completely screened 10 nm size gold nanoparticles below it. In spite of sufficient difference in atomic number, gold became 'invisible' beneath the chromium, apparently, because of relatively thick and coarse morphology of the latter. But, when gold nanoparticle dispersion was deposited on a glass precoated with 50 nm thick Cr layer, the separate nanoparticles and their groups were clearly observed, as shown in Figure 2(B).

In the conventional configuration of metallic coating, the film thickness should be thinner than the height of the particles in order to reveal small nanoparticles. However, if the film is too thin, it becomes discontinuous and decorates the sample (Peters, 1986). Since the surface topography of biological tissues is rather complex, ultrathin coatings of 1–2 nm are less suitable to provide a continuous layer across large areas of the sample (Stokroos *et al.*, 1998). Therefore, the suggested configuration of a conductive layer, as a substrate rather than as a coating, provides a solution to the charging problem of nonconductive samples and allows the observation of nanometric elements, as shown in further experiments.

HRSEM observation of gold nanoparticles in cells

Macrophages cells were cultured on a glass substrate coated with 50 nm chromium and incubated with 1% dilution of 30 nm gold nanoparticles stock solution for 2 h. Figure 3 compares between BSE and SE images of a single macrophage, taken at 5 kV. At BSE mode, the conductive layer below the cell minimizes the charging of the biological specimen and allows detection of a single gold nanoparticle (Fig. 3A, C). However, in SE mode, the charging is still significant, yielding a poor image quality and masking the signal from the gold nanoparticle (Fig. 3B, D). Because BSE are high in energy compared to SE they are less sensitive to local electrostatic fields caused by the charging (Walther *et al.*, 1991). In addition, for low atomic number materials, such as biological tissue, the SE imaging is limited by the low SE yield. As the incident probe size is decreased, the current in the probe may fall below the threshold value required for imaging. Increase in the accelerating voltage results in more pronounced charging of the nonconductive biological specimen (Joy, 1996). Nevertheless, the large difference between the low atomic number of the

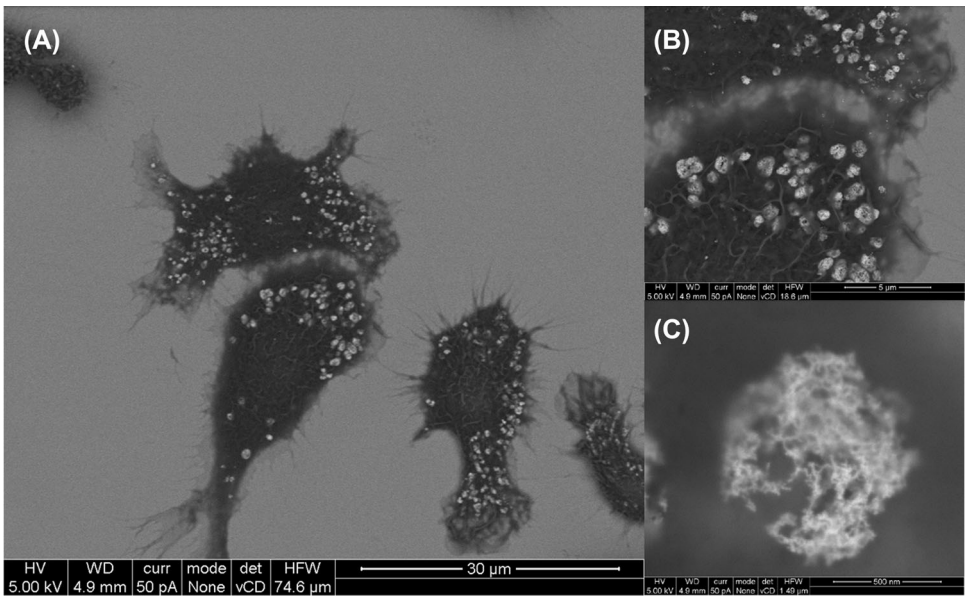

Fig. 4. BSE images of macrophages incubated with 50% dilution of 10 nm-sized gold NPs over 13 h on glass coated with Cr 50 nm layer. Images 'B' & 'C' are higher magnifications of 'A'.

biological cells and the high atomic number of gold nanoparticles makes the BSE signal the right choice for imaging in our study.

In another experiment, macrophages were cultured on glass coated with chromium and incubated with 50% concentration of 10 nm gold nanoparticles stock solution over 13 h. Figure 4(A) shows a general view of several macrophages imaged in BSE, wherein clusters of gold nanoparticles can be easily observed. At higher magnification (Fig. 4B,C), it can be seen that the nanoparticles are grouped together inside spherical vesicles, each containing hundreds of nanoparticles. The uptake of gold nanoparticles in macrophages cells occurs by an endocytotic pathway; internalization in lysosomes and perinuclear arrangement, as studied by AFM, CFLSM and TEM (Shukla *et al.*, 2005). The advantage of HRSEM is the ability to scale down and study the arrangement of nanometric elements in their wider context. This makes the technique simpler and more intuitive. In addition, the ability to observe the whole cell rather than cross sections, as required for TEM, simplifies the process of sample preparation.

In subsequent experiments, we studied the kinetics of 10 nm gold nanoparticles uptake by macrophages by BSE imaging. Cells were cultured on glass coated with chromium and incubated with 50% concentration of 10 nm gold nanoparticle for 0.5, 2.5 and 22 h, as shown in Figure 5. At the short time of 0.5 h, only single or very small groups of nanoparticles were detected. After a longer exposure of 2.5 h, larger groups of nanoparticles were observed. At the longest incubation time of 22 h, an impressive uptake of gold nanoparticles was observed, showing closely packed dense vesicles, containing hundreds of nanoparticles.

The advantage of imaging in back-scattered electrons is its ability to penetrate the organic material and to show a signal from gold nanoparticles located inside the cells. NPs located closer to the surface of the cell possess stronger BSE signal and therefore appear brighter in the image. Figure 6(A) demonstrates clusters of nanoparticles located at different depths of the cell. The sharp and detailed spheres represent nanoparticles that are on the surface of the cell or very close to it, whereas the hazy spheres represent nanoparticles that are deeper inside. Figure 6(B) shows at a higher magnification a cluster of NPs that is partially inside the cell and partially outside. The depth of the NPs below the surface of the cell can be calculated from BSE imaging. This was not implemented in our study, however we refer the readers to the very recent work by Seiter *et al.* (2014). In their study, BSE images were taken at untilted and tilted sample positions and the depth of the inner particles was calculated using a triangulation method. In another method, they determined the minimum primary electron energy at which the NPs can be still recognized and calculated the depth using the Kanaya-Okayama model (Kanaya & Okayama, 1972).

Figure 6(C) demonstrates the ability to distinguish between each individual 10 nm nanoparticle, comprising a chain of gold nanoparticles. Overcoming the problem of specimen charging makes it possible to take advantage of the very high resolution of the extra-HRSEM tool. It allows the study of the specific spatial arrangement of nanoparticles and thus the examination of possible interactions between them.

SE signal is generated at or very close to the surface of the specimen, whereas that of BSE is less surface-specific and

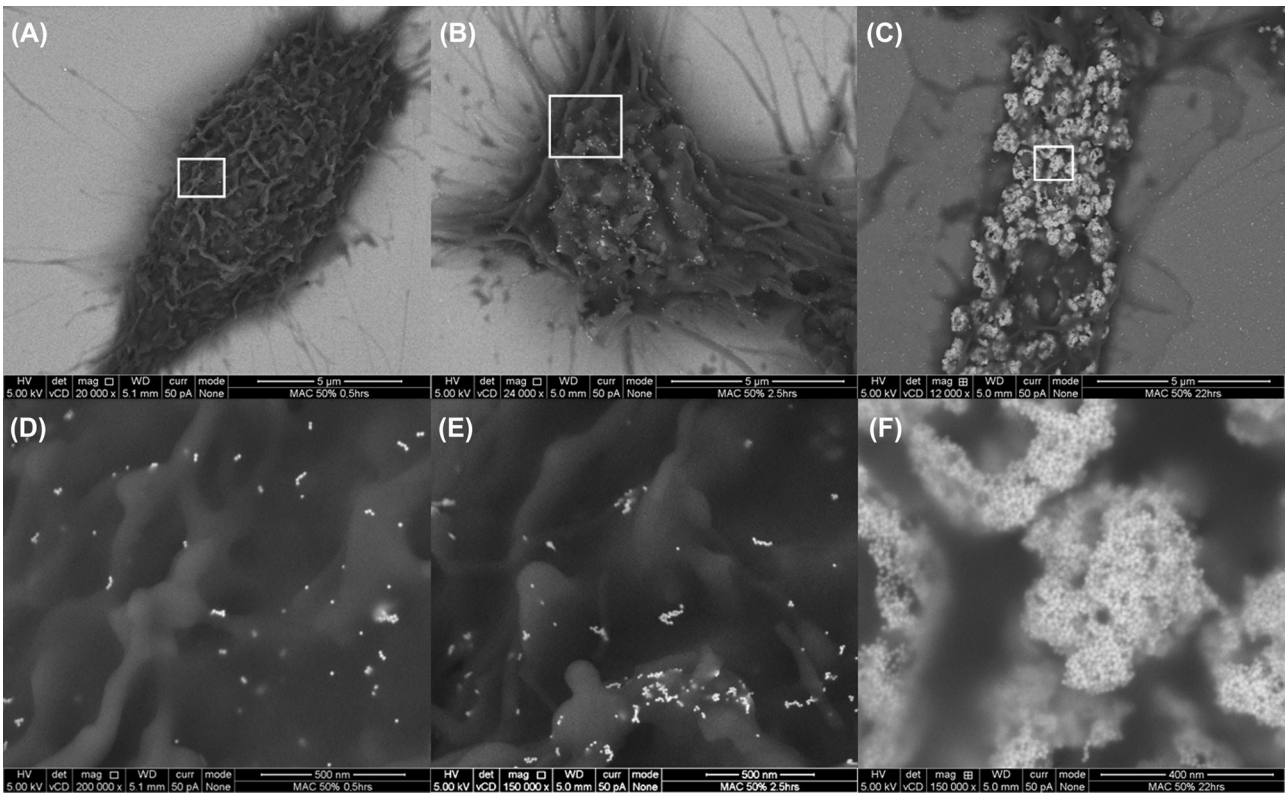

Fig. 5. BSE images of macrophages incubated on Cr coated glass with 50% dilution of 10 nm-sized gold NPs over different incubation periods: (A) 0.5 h, (B) 2.5 h, (C) 22 h. 'D', 'E' & 'F' are enlargements of the ROI marked with a rectangle in 'A', 'B' & 'C', respectively.

carries information from depths of the specimen (Joy, 1996). Therefore, a comparison between SE and BSE images acquired at the same region may be used as a tool to determine whether the nanoparticles are on the surface or inside the cell. Figure 7 shows BSE and SE images of two adjacent HaCaT cells, that were incubated with 50% concentration of 10 nm gold NPs for 22 h. The clusters of gold nanoparticles in the BSE image (Fig. 7A) appear very bright, which gives the impression that they are out of the cells. The SE image (Fig. 7B) clarifies that most of the clusters are covered by an organic material, therefore located inside the cells. A few clusters on the left corner appear very bright also in the SE image, which may indicate their location on the surface of the cell. The presence of gold nanoparticles clusters on top of or very close to the cell membrane, suggests that the aggregates of gold nanoparticles were already formed inside the medium. This finding is also supported by the change of the medium colour with incubation time, from pink to dark red (not shown). According to the study of Park *et al.*, gold nanoparticles form aggregates in RPMI medium containing 10% FBS serum mainly due to the adsorption of the serum to the gold surface, and are internalized in an aggregation state in mammalian cells (Park *et al.*, 2011).

HRSEM observation of gold nanoparticles in tissue

The application of a conductive substrate was also implemented on a tissue culture. Skin cryo-sections of treated skin samples were placed on a glass coated with chromium layer. Figure 8(A) shows the cutting edge of a skin cross-section in a sample that was incubated with 5 nm gold nanoparticles in the medium. Fibres of the dermis are seen on top of a wavy background. It is evident that the nonconductive serum coating, that was applied to the chromium layer in order to improve adhesion, masks the conductivity of the chromium layer and the sample suffers from a significant charging, which appears as dark waves at the background. The fibres of the dermis are also electrically charged as can be seen by their bright reflectance. Some groups of gold nanoparticles were observed on the fibres of the dermis at the very edge. However, the quality of the image was not good enough to locate additional nanoparticles deeper along the section. Figure 8(B) shows a skin cross-section of a sample that was smeared topically with gold nanoparticles. It is evident that the whole piece of skin tissue was electrically charged, which makes it impossible to distinguish between the different parts of the tissue. Some hazy bright spot on *the stratum corneum* suggest the existence of gold nanoparticles. However, the quality

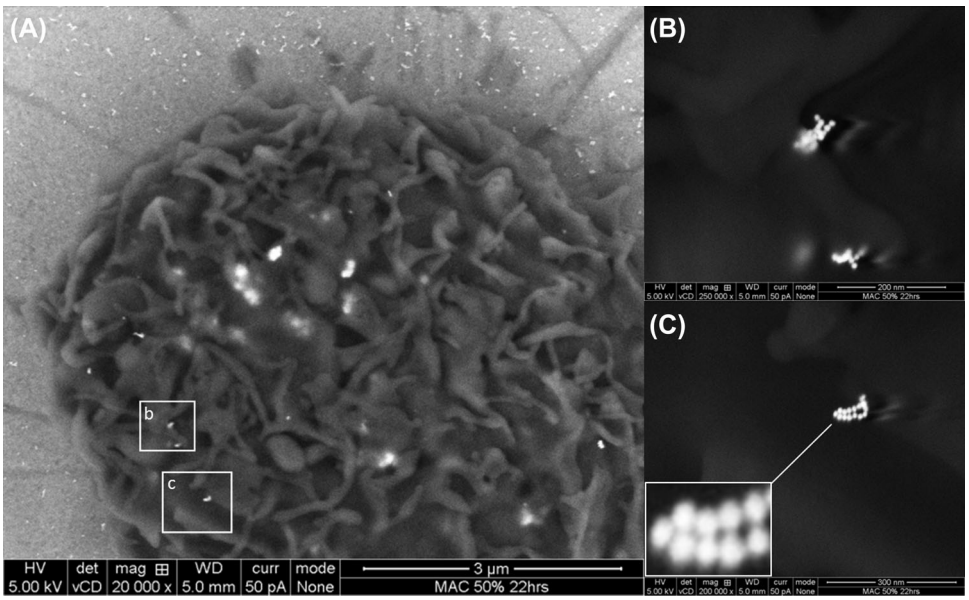

Fig. 6. BSE images of a macrophage incubated with 50% dilution of 10 nm-sized gold nanoparticles for 22 h on glass coated with Cr 50 nm layer. (A) clusters of NPs in different depths of the cell. (B) clusters of NPs partially in and partially out of the cell. (C). A 'chain' of 10 nm-sized gold nanoparticles with a zoom-in by a factor of five in the small rectangle, that demonstrates the ability to resolve between adjacent nanoparticles.

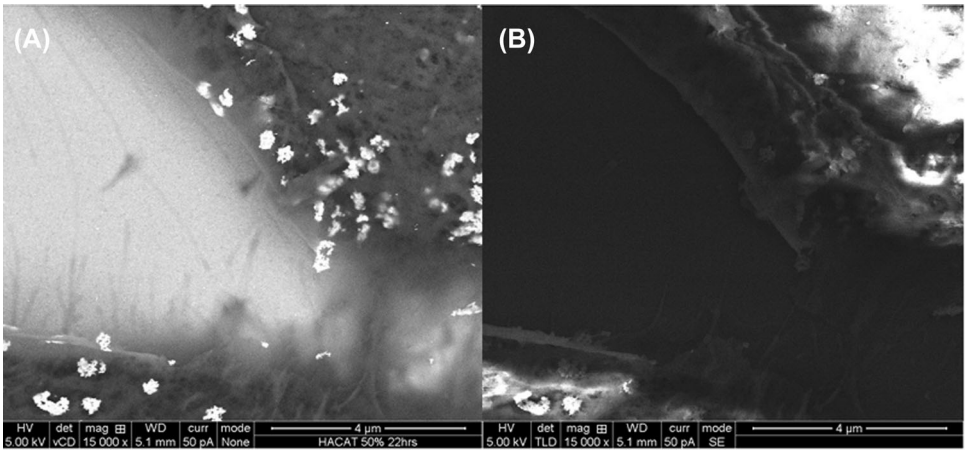

Fig. 7. A comparison between BSE image (A) and SE image (B) of HaCaT cell, incubated with 50% dilution of 10 nm-sized gold nanoparticles for 22 h on glass coated with Cr 50 nm layer. Most of the bright clusters of NPs that appear at the BSE mode are missing at the SE mode, indicating their subsurface location.

of the image was not good enough for analysis at a higher magnification.

In order to improve the conductivity of the biological tissue sample, a method to avoid the use of the serum layer was developed. Since the serum is required to improve adhesion between the tissue and the sample holder during the washing stages of the ethanol-freon dehydration method, this procedure was excluded and the samples were dried in an oven instead. The absence of the serum reduced the charging but did not eliminate it completely (not shown). In order to further improve the conductivity of the sample holder, pieces of silicon substrate were coated with a stack of 50 nm chromium layer and 1 μm thick copper. The combination of a semiconductor substrate and a metallic layer with an excellent electrical conductivity produced a highly conductive sample holder that is critical for the observation of rather large nonconductive specimen by SEM. The alternative dehydration procedure makes it possible to mount the biological sample directly on top of the conductive metal without using the nonconductive serum in between. In this setup, since the skin section is mounted on top of the holder after fixation, the toxicity of the copper layer is not an issue. Figure 9(A) shows a general view of the skin cross-section that was placed on the improved conductive substrate. Charging effect was considerably reduced and the

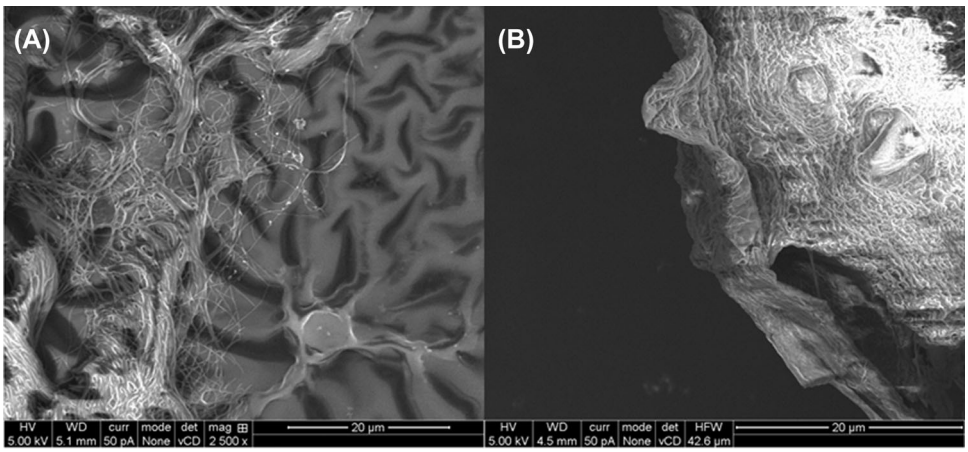

Fig. 8. BSE images of skin cross sections on serum/Cr/glass holders: (A) The bottom edge of skin cross-section treated by AuNPs in the medium 10 nm. Charging of the nonconductive serum at the background of the dermis fibres is observed, (B) the upper part of skin cross section topically treated by AuNPs 10 nm; over-brightness in the upper right part of the cross-section originates from the strong charging.

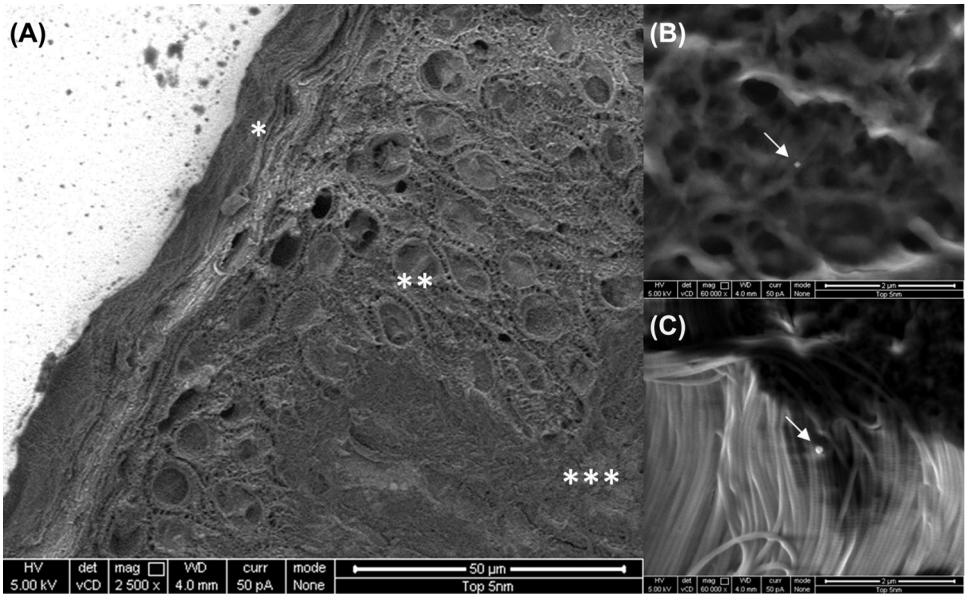

Fig. 9. BSE of a skin cross-section mounted on a highly conductive Cu/Si holder. Skin was smeared topically with 5 nm AuNPs for 24 h: (A) a general view of the skin cross section showing the different layers of the skin: **stratum corneum*, ** epidermis, *** dermis, (B) a cluster of gold nanoparticles 40 microns deep inside the epidermis, (C) a cluster of gold nanoparticles 300 microns deep inside the dermis.

different layers of the skin could be easily observed (Fig. 9A). The improved conditions made it possible to scan the samples and locate gold nanoparticles inside the different part of the skin. Figure 9(B) is a representative image of a group of nanoparticles located in the epidermis and Fig. 9(C) in the dermis.

This experiment showed that topically applied 5 nm gold nanoparticles penetrate through the barrier of the *stratum corneum*, into the epidermis and even deeper in to the dermis. Nanoparticles were found over 500 microns deep into the skin. It should be noted that the complicated sample environment of a skin cross-section does not allow obtaining a 5 nm resolution. The nanoparticles that were observed inside the epidermis and dermis were in fact aggregates of several NPs together, usually 50–150 nm size. It is very likely to assume that at the penetration depth of large aggregates there were also single NPs which weren't observed due to the sample limitations. Monitoring of nanoparticles penetration into the skin is very challenging. The aim of our study was to qualitatively assess whether 5 nm sized AuNPs penetrate the skin and to which layer. The imaging results indicate that HRSEM may be used as a relatively simple tool for qualitative screening of the factors that enhance AuNPs penetration, through the skin barrier. In order to quantify

the number of nanoparticles penetration through the *stratum corneum*, other approaches should be applied, such as diffusion cells (Filon *et al*., 2011) and multiphoton microscopy (Labouta *et al*., 2013).

Conclusions

Equipment of the scanning electron microscope has evolved significantly in the recent years and can now reach a resolution better than 1 nm. The advantages of using SEM are numerous and include the ability to view the object of interest at low and high magnification, viewing the entire object rather than a cross-section, simple and more intuitive analysis of the images, giving 3D information on structure and morphology and evidently a much simpler sample preparation process. In order to overcome charging artefact related to nonconductive biological materials, an alternative configuration of conductive sample setup was demonstrated. By growing cells on glass precoated with a conductive chromium layer, we were able to observe the uptake of 10 nm gold nanoparticles inside uncoated and unstained macrophages and keratinocytes cells. Chromium coating, as well as tantalum and titanium/tungsten, were shown to be nontoxic, with similar cell growth compared to conventional glass microscopy slides. Imaging in back-scattered electrons allowed observation of gold nanoparticles located in vesicles inside the cells, while imaging with secondary electrons gave information on gold nanoparticles located on the surface of the cells and was more sensitive to charging artefact. A kinetic study was carried out on macrophages, showing the uptake of single nanoparticles after a short incubation period of 0.5 h, larger clusters after 2.5 h and an impressive uptake after 22 h. The configuration of a conductive holder was successfully implemented to the observation of skin culture. The relatively large nonconductive specimen of the skin tissue was more challenging in terms of charging elimination. For that purpose, an improved conductive sample holder was produced, consisting of a silicon substrate coated with copper. With the new setup we were able to observe an uncoated skin cross-section and to qualitatively evaluate the penetration of 5 nm gold nanoparticles through the skin barrier. With the emerging research of nanotechnology in biological application, HRSEM may provide a powerful and diverse tool for the study of the interactions between biological systems and metallic nanostructures. The suggested simplified procedure for sample preparation may be of use to other researchers that wish to obtain qualitative results in a quick and simple manner using standard accessible equipment.

Acknowledgements

This research was supported in part by the chief scientist of the Israeli Ministry of Health. We would like to thank Dr. Douglas Gilliland for his assistance with the supply of 10 and 30 nm gold nanoparticles. The nanoparticles were prepared and supplied by the Joint Research Centre of the European Commission using methods developed within the European Union Seventh Framework Programme (FP7/2007–2013) under grant agreement no. 214478 (NanoReTox). AVX Israel Ltd. is gratefully acknowledged for the Sputtering of the metallic thin films on glass cover slips.

References

Bogner, E., Dominizi, K., Hagl, P., Bertagnolli, E., Wirth, M., Gabor, F., Brezna, W. & Wanzenboeck, H. D. (2006) Bridging the gap–biocompatibility of microelectronic materials. *Acta Biomater* **2**, 229–237.

Brunk, U., Collins, P. & Arro, E. (1980) The fixation, dehydration, drying and coating of cultured cells for SEM. *J Microsc* **123**, 121–131.

Denk, W. & Horstmann, H. (2004) Serial block-face scanning electron microscopy to reconstruct three-dimensional tissue nanostructure. *PLoS Biol* **2**, e329.

Dreaden, E. C., Alkilany, A. M., Huang, X., Murphy, C. J. & El-Sayed, M. A. (2012) The golden age: gold nanoparticles for biomedicine. *Chem Soc Rev* **41**, 2740–2779.

Filon, F. L., Crosera, M., Adami, G., Bovenzi, M., Rossi, F. & Maina, G. (2011) Human skin penetration of gold nanoparticles through intact and damaged skin. *Nanotoxicology* **5**, 493–501.

Goldstein, J. (1981) *Scanning Electron Microscopy and X-Ray Microanalysis*, Plenum Press, New York, NY.

Hartsuiker, L., VAN Es, P., Petersen, W., VAN Leeuwen, T. G., Terstappen, L. W., Otto, C. (2011) Quantitative detection of gold nanoparticles on individual, unstained cancer cells by scanning electron microscopy. *J Microsc* **244**, 187–193.

Huang, X., Jain, P. K., El-Sayed, I. H. & El-Sayed, M. A. (2007) Gold nanoparticles: interesting optical properties and recent applications in cancer diagnostics and therapy. *Nanomedicine (Lond)* **2**, 681–693.

Hughes, L., Hawes, C., Monteith, S. & Vaughan, S. (2013) Serial block face scanning electron microscopy–the future of cell ultrastructure imaging. *Protoplasma* **251**, 395–401.

Joy, D. C. (1991) The theory and practice of high-resolution scanning electron-microscopy. *Ultramicroscopy* **37**, 216–233.

Joy, D. & Joy, C. (1996) Low voltage scanning electron microscopy. *Micron* **27**, 247–263.

Joy, D. C. & Pawley, J. B. (1992) High-resolution scanning electron microscopy. *Ultramicroscopy* **47**, 80–100.

Kanaya, K. & Okayama, S. (1972) Penetration and Energy-Loss Theory of Electrons in Solid Targets. *Journal of Physics D-Applied Physics* **5**, 43–58.

Labouta, H. I., Thude, S. & Schneider, M. (2013) Setup for investigating gold nanoparticle penetration through reconstructed skin and comparison to published human skin data. *J Biomed Opt* **18**, 061218.

Levy, R., Shaheen, U., Cesbron, Y. & See, V. (2010) Gold nanoparticles delivery in mammalian live cells: a critical review. *Nano Rev* **1**. doi: 10.3402/nano.v1i0.4889

Mosmann, T. (1983) Rapid colorimetric assay for cellular growth and survival: application to proliferation and cytotoxicity assays. *J Immunol Methods* **65**, 55–63.

Park, J., Park, J. H., Ock, K. S., Ganbold, E. O., Song, N. W., Cho, K., Lee, S. Y. & Joo, S. W. (2011) Preferential adsorption of fetal bovine serum on bare and aromatic thiol-functionalized gold surfaces in cell culture media. *J Colloid Interface Sci* **363**, 105–113.

Peters, K. R. (1986) Rationale for the application of thin, continuous metal films in high magnification electron microscopy. *J Microsc* **142**, 25–34.

Plascencia-Villa, G., Bahena, D., Rodriguez, A. R., Ponce, A. & Jose-Yacaman, M. (2013) Advanced microscopy of star-shaped gold nanoparticles and their adsorption-uptake by macrophages. *Metallomics* **5**, 242–250.

Pluk, H., Stokes, D. J., Lich, B. & Wieringa, B. (2008) Advantages of indium-tin oxide-coated glass slides in correlative scanning electron microscopy applications of uncoated cultured cells. *J Microsc* **233**, 353–363.

Prausnitz, M. R., Mitragotri, S. & Langer, R. (2004) Current status and future potential of transdermal drug delivery. *Nat Rev Drug Discov* **3**, 115–124.

Rajani, K. V., Daniels, S., McNally, P. J., Lucas, F. O. & Alam, M. M. (2010) Ultrathin chromium transparent metal contacts by pulsed dc magnetron sputtering. *Physica Status Solidi a-Applications and Materials Science* **207**, 1586–1589.

Robinson (1975) Elimination of chargingartifacts in scanning electron-microscope. *J. Phys. E: Sci. Instrum* **8**, 638–640.

Rouvinski, A., Karniely, S., Kounin, M., *et al.* (2014) Live imaging of prions reveals nascent PrPSc in cell-surface, raft-associated amyloid strings and webs. *J Cell Biol* **204**, 423–441.

Ryman-Rasmussen, J. P., Riviere, J. E. & Monteiro-Riviere, N. A. (2006) Penetration of intact skin by quantum dots with diverse physicochemical properties. *Toxicol Sci* **91**, 159–165.

Schatten, H. (2010) Low voltage high-resolution SEM (LVHRSEM) for biological structural and molecular analysis. *Micron* **42**, 175–185.

Schrand, A. M., Schlager, J. J., Dai, L. & Hussain, S. M. (2010) Preparation of cells for assessing ultrastructural localization of nanoparticles with transmission electron microscopy. *Nat Protoc* **5**, 744–757.

Seiter, J., Muller, E., Blank, H., Gehrke, H., Marko, D. & Gerthsen, D. (2014) Backscattered electron SEM imaging of cells and determination of the information depth. *Journal of Microscopy* **254**, 75–83.

Shukla, R., Bansal, V., Chaudhary, M., Basu, A., Bhonde, R. R. & Sastry, M. (2005) Biocompatibility of gold nanoparticles and their endocytotic fate inside the cellular compartment: a microscopic overview. *Langmuir* **21**, 10644–10654.

Sonavane, G., Tomoda, K., Sano, A., Ohshima, H., Terada, H. & Makino, K. (2008) In vitro permeation of gold nanoparticles through rat skin and rat intestine: effect of particle size. *Colloids Surf B Biointerfaces* **65**, 1–10.

Stokroos, I., Kalicharan, D., Van Der Want, J. J. & Jongebloed, W. L. (1998) A comparative study of thin coatings of Au/Pd, Pt and Cr produced by magnetron sputtering for FE-SEM. *J Microsc* **189**, 79–89.

Summers, H. D., Brown, M. R., Holton, M. D., Tonkin, J. A., Hondow, N., Brown, A. P., Brydson, R. & Rees, P. (2013) Quantification of nanoparticle dose and vesicular inheritance in proliferating cells. *ACS Nano* **7**, 6129–6137.

Titze, B. & Denk, W. (2013) Automated in-chamber specimen coating for serial block-face electron microscopy. *J Microsc* **250**, 101–110.

Walther, P., Autrata, R., Chen, Y. & Pawley, J. B. (1991) Backscattered Electron Imaging for High-Resolution Surface-Scanning Electron-Microscopy with a New Type Yag-Detector. *Scanning Microscopy* **5**, 301–310.

Wolbers, F., ter Braak, P., Le Gac, S., Luttge, R., Andersson, H., Vermes, I. & van den Berg, A. (2006) Viability study of HL60 cells in contact with commonly used microchip materials. *Electrophoresis* **27**, 5073–5080.